Star-forming, rotating spheroidal galaxies in the GAMA and SAMI surveys

Amanda J. Moffett,[1,2]⋆ Steven Phillipps [ID],[3] Aaron S. G. Robotham [ID],[4]
Simon P. Driver,[4] Malcolm N. Bremer,[3] Luca Cortese [ID],[4,5] O. Ivy Wong,[4]
Sarah Brough [ID],[6] Michael J. I. Brown [ID],[7] Julia J. Bryant,[5,8,9] Christopher J. Conselice,[10]
Scott M. Croom [ID],[5,6] Koshy George [ID],[11,12] Greg Goldstein,[13] Michael Goodwin,[9]
Benne W. Holwerda [ID],[14] Andrew M. Hopkins,[15] Iraklis S. Konstantopoulos,[16]
Jon S. Lawrence,[15] Nuria P. F. Lorente,[9] Anne M. Medling [ID],[17,18]† Matt S. Owers,[12]
Kevin A. Pimbblet,[19] Samuel N. Richards [ID],[20] Sarah M. Sweet [ID][5,21]
and Jesse van de Sande [ID][5,8]

Affiliations are listed at the end of the paper

ABSTRACT

The Galaxy And Mass Assembly (GAMA) survey has morphologically identified a class of 'Little Blue Spheroid' (LBS) galaxies whose relationship to other classes of galaxies we now examine in detail. Considering a sample of 868 LBSs, we find that such galaxies display similar but not identical colours, specific star formation rates, stellar population ages, mass-to-light ratios, and metallicities to Sd-Irr galaxies. We also find that LBSs typically occupy environments of even lower density than those of Sd-Irr galaxies, where $\sim$65 per cent of LBS galaxies live in isolation. Using deep, high-resolution imaging from VST KiDS and the new Bayesian, 2D galaxy profile modelling code PROFIT, we further examine the detailed structure of LBSs and find that their Sérsic indices, sizes, and axial ratios are compatible with those of low-mass elliptical galaxies. We then examine SAMI Galaxy survey integral field emission line kinematics for a subset of 62 LBSs and find that the *majority* (42) of these galaxies display ordered rotation with the remainder displaying disturbed/non-ordered dynamics. Finally, we consider potential evolutionary scenarios for a population with this unusual combination of properties, concluding that LBSs are likely formed by a mixture of merger and accretion processes still recently active in low-redshift dwarf populations. We also infer that if LBS-like galaxies were subjected to quenching in a rich environment, they would plausibly resemble cluster dwarf ellipticals.

Key words: surveys – galaxies: dwarf – galaxies: fundamental parameters – galaxies: structure.

1 INTRODUCTION

In the last three decades, increasingly large samples of galaxies have been surveyed in terms of their photometric and spectroscopic properties (e.g. 2dFGRS, Colless et al. 2001; SDSS, York et al. 2000; GAMA, Driver et al. 2009). Such surveys have provided the means to quantify the characteristic properties of different classes

of galaxies, and a primary method of dividing galaxies into classes with similar characteristics is through morphological classification. The interest in galaxy morphology is motivated in part by the apparent link between a galaxy's structure and its likely formation history, with spheroidal structures generally thought to result from dissipationless processes such as dry mergers (e.g. Cole et al. 2000) and disc-like structures thought to result from dissipational gas physics processes (e.g. Fall & Efstathiou 1980). While it is likely that the dynamics of a galaxy provide a more direct probe of their formation histories, morphological classification has one advantage in its feasibility for significantly larger populations of galaxies.

⋆ E-mail: amanda.moffett@ung.edu
† Hubble Fellow.

The large-scale morphological classification of survey samples include work carried out by survey teams themselves (e.g. Kelvin et al. 2014, Moffett et al. 2016a), by 'citizen scientists,' as in the Galaxy Zoo project (e.g. Lintott et al. 2011, Willett et al. 2013), and through automated classification schemes such as CAS (Conselice 2003), Gini-M20 (Lotz, Primack & Madau 2004), and deep learning algorithms (Huertas-Company et al. 2015). Such work has presented an opportunity to identify new or rare types of galaxies, for instance the SDSS discoveries of 'Green Peas' (Cardamone et al. 2009) and isolated compact ellipticals (Huxor, Phillipps & Price 2013).

Another recently identified class of galaxy is the blue but morphologically early-type galaxy, which includes the blue ellipticals of Driver et al. (2006) and the blue E/S0s of Kannappan, Guie & Baker (2009) and Schawinski et al. (2009). Here we discuss another such class of galaxies known as the 'little blue spheroids' (LBS) identified in the Galaxy And Mass Assembly (GAMA) survey. Note that each of these classes are likely to differ in detailed properties due to the differing limits and selections of their origin samples. In particular, the mass ranges of these blue early-type populations differ significantly, where the Schawinski et al. (2009) population are approximately L^* galaxies, the Kannappan et al. (2009) population reaches into the dwarf mass regime with stellar mass $\sim 10^8 \, M_\odot$, and GAMA's LBS extend down to stellar mass $\sim 10^7 \, M_\odot$.

These blue early-type galaxies may also overlap with the well-studied, nearby blue compact dwarf (BCD) galaxy population (Thuan & Martin 1981), which although identified in a number of ways by different authors, share the characteristics of being blue (typically judged via optical colour of the core), compact (judged by high B-band surface brightness of the core), and dwarf (low mass but often traced by an optical luminosity cut; Gil de Paz, Madore & Pevunova 2003). These requirements can select for galaxies with morphological similarity to the aforementioned blue early types, however observed BCDs come in a variety of shapes, from those that appear as a purely spheroidal core to those with both smooth and clumpy outer envelopes (see e.g. Loose & Thuan 1986; Gil de Paz et al. 2003).

As part of the GAMA survey, visual morphological classifications were completed for a sample of galaxies out to $z = 0.06$, by utilizing three-colour (giH) postage-stamp images. Among these objects, Kelvin et al. (2014) identified a class that they called 'little blue', which appeared to lie outside the expected range of morphological types. This class of galaxies was defined by the multiple observer visual impression of compact and round morphology along with blue colour (also judged visually) and comprised 7.4 per cent of the classified sample. Moffett et al. (2016a) subsequently expanded this visual morphology classification using the same visual classifiers of Kelvin et al. (2014) and approximately doubled the sample size by extending to a larger GAMA phase two sample with a fainter magnitude limit ($r < 19.8$ compared to $r < 19.4$ mag) and a larger sky area ($180 \, \mathrm{deg}^2$ compared to $144 \, \mathrm{deg}^2$). LBS galaxies made up 11.5 per cent of this expanded sample, which contained a larger proportion of faint/lower mass objects. Moffett et al. (2016b) also estimated that these galaxies make up around 1 per cent of the total low redshift stellar mass in GAMA. Note that since this classification is based purely on galaxy images as they are observed with a variety of on-sky projection angles, LBS galaxies may or may not actually represent spheroids in three dimensions. We treat the structural and dynamical similarity of this LBS class to spheroidal galaxies as a matter of investigation in this work.

The closest relatives to these LBS galaxies may be 'normal' dwarf elliptical, or dE, galaxies, which share their apparent spheroidal appearance but typically not their blue colour. Dwarf elliptical galaxies are distinguished from their giant elliptical counterparts not only by virtue of lower mass (or fainter magnitude) but also by a profile shape that is typically more shallow, closer to an exponential profile than the steep de Vaucouleurs profile characteristic of giant ellipticals (e.g. Faber & Lin 1983; Binggeli, Sandage & Tarenghi 1984; Sandage & Binggeli 1984; Ferguson & Binggeli 1994). Much like a giant elliptical, a typical dE galaxy appears red in optical three-colour images similar to those used for classification in the GAMA survey (see e.g. Buta 2013 for examples), and most dEs are characterized by old stellar population ages with little evidence for recent star formation. Most known dEs are also found in relatively rich environments, and dEs have been found to be the most numerous type of galaxy in several galaxy clusters (see review of Ferguson & Binggeli 1994 and references therein).

In this paper we explore the detailed properties of the galaxies classified as LBSs. We compare these to the properties of other types of low-mass galaxies in order to investigate the current and past relationship between LBSs and other classes of low-mass galaxies. We first introduce our sample and data in Section 2. We then consider the basic properties of LBS galaxies as derived from various GAMA-based catalogues in Section 3, finding a strong similarity in stellar population properties and environments between GAMA LBSs and Sd-Irrs. We next analyse the detailed structural properties of LBSs using deep, high-resolution optical imaging from the VST KiDS survey (de Jong et al. 2013) in Section 4. We find that LBSs have quantitatively similar structure to low-mass ellipticals as might be expected from their qualitatively judged morphology. We then examine the emission line kinematics of a subsample of LBSs observed by the SAMI Galaxy survey (Croom et al. 2012) in Section 5, finding that contrary to the expectation from their spheroid-like structure, most LBSs are at least marginally rotation-dominated galaxies. Finally in Section 6 we summarize our results and discuss their implications for the likely origins and future evolution of LBS galaxies, concluding that LBSs likely emerge from a mixture of galaxy–galaxy interaction and accretion processes and could form a plausible progenitor population for dwarf ellipticals.

Throughout this work we use a standard concordance cosmology, i.e. $H_0 = 70 \, \mathrm{km \, s^{-1} \, Mpc^{-1}}$, $\Omega_m = 0.3$, $\Omega_\Lambda = 0.7$, as in other GAMA data products.

2 GAMA SAMPLE AND DATA PRODUCTS

The GAMA survey is a combined spectroscopic and multiwavelength imaging survey of five patches of the sky, with total area 286 square degrees, down to a magnitude limit of $r = 19.8$, with spectroscopic observations from the AAO mega spectrograph on the Anglo-Australian Telescope (see Liske et al. 2015 for a recent summary of GAMA Data Release 2). The three GAMA equatorial regions, amounting to a total sky area of $180 \, \mathrm{deg}^2$, were selected for this study due to the availability of visual morphology classifications and spectroscopic redshift survey completeness >98 per cent to $r < 19.8$ mag (Liske et al. 2015). The survey was based originally on catalogued SDSS photometry, but this has since been reprocessed and homogenized to give improved magnitudes (Hill et al. 2011; Wright et al. 2016). In addition to the basic photometric data and the survey's spectroscopic data (Hopkins et al. 2013), GAMA catalogues also provide a wide range of derived properties (as described by Liske et al. 2015), such as stellar population and dust extinction parameters, inferred masses, and mass-to-light ratios (Taylor et al. 2011; Wright et al. 2016), star formation rates (e.g.
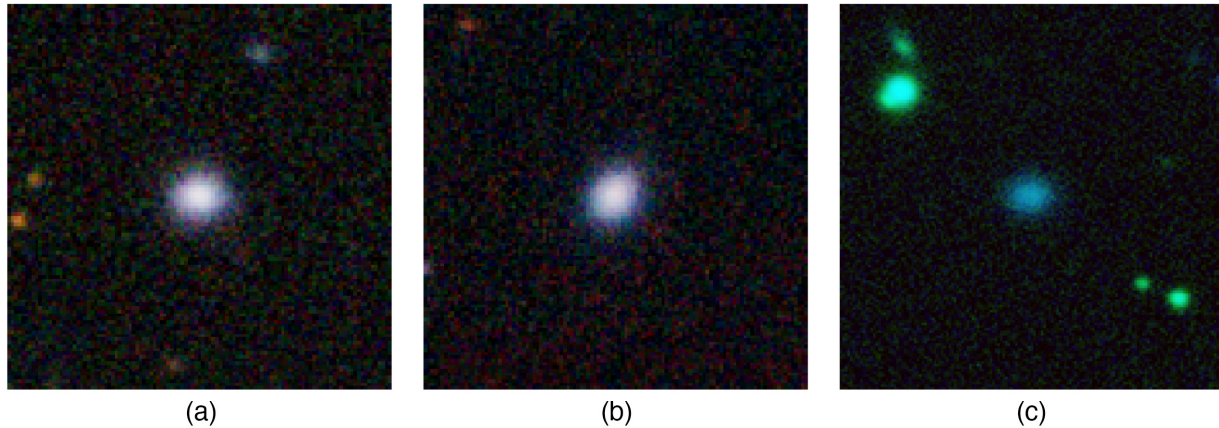
Figure 1. Representative LBS galaxies (GAMA IDs G300372, G418795, and G417568) in their original three-colour (*giH*) classification images. Classification images are 30 kpc on a side in size (Moffett et al. 2016a), and all images are scaled using the same algorithm (tanh scaling) such that scaling differences reflect the changing dynamic range in each image (for example, the scaling in the far right panel is affected by a nearby bright point source).

Davies et al. 2016, Wright et al. 2016) and environmental measures (e.g. Robotham et al. 2011).

The primary defining subsample for this paper is the GAMA-II visual morphology catalogue, which consists of 7556 objects in the GAMA equatorial regions with local flow-corrected redshifts in the range of $0.002 < z < 0.06$, normalized redshift quality nQ > 2 (i.e. good for science),[1] and extinction-corrected SDSS *r* band Petrosian magnitude of $r < 19.8$ mag (see Moffett et al. 2016a for further details). In the GAMA visual morphology analysis, galaxies are classified into broad galaxy classes based primarily on their spheroid-/disc-dominated appearance and then their single-/multicomponent nature (yielding broad classes E, S0-Sa, SB0-SBa, Sab-Scd, SBab-SBcd, Sd-Irr, and LBS) via the consensus of a team of human classifiers (see fig. 2 of Moffett et al. 2016a for examples of each class). Note that the presence or absence of any tidal feature/disturbance is not a criterion of this classification scheme, so in the case of merging systems each galaxy distinguishable as a separate GAMA object is separately classified according to the aforementioned scheme. Moffett et al. (2016a) classify 868 total galaxies as LBSs, which is the full sample of LBSs we consider here (see example LBS classification images in Fig. 1).[2]

In subsequent sections we explore the properties of LBSs in order to investigate the defining characteristics of the LBS class. We use a variety of GAMA catalogue data on the LBSs and other low-mass GAMA galaxies in order to explore differences and similarities in the parameter distributions amongst them. To this end, we consider

GAMA-derived stellar population parameters including colours and star formation rates, plus environments. We then extend the study to more detailed consideration of the structure and kinematics of LBSs. Specifically, improved optical imaging data are now available from the KiDS survey (de Jong et al. 2013) and we use this to determine the detailed structural characteristics of the LBSs, in terms of both single and two-component Sérsic fits. These fits are then compared to similar structural fits of other galaxy types. We also consider integral field spectroscopic observations for a subsample of LBS galaxies with data available in the SAMI Galaxy survey data release 2 (Croom et al. 2012; Bryant et al. 2015; Scott et al. 2018) to assess whether these galaxies display primarily rotation- or dispersion-dominated kinematics.

3 GAMA-DERIVED PROPERTIES OF LBS GALAXIES

We first compare the basic parameters of LBSs to those of other morphologically defined galaxy classes. In total 868 galaxies are classified as LBS in our visual morphology catalogue, and Fig. 2 shows their position in a $g - i$ colour versus stellar mass diagram compared to the other galaxy types. It is evident that they largely occupy the region towards the low-mass end of the blue cloud, though a few may lie on the extension of the red sequence to low mass if the spread in colour is not simply due to random error. To first order, then, it seems that the large majority of LBSs should be generically similar to faint late-type galaxies (both being 'little' and 'blue'). Further, in previous studies of GAMA dwarfs that have included members of the LBS population, such galaxies have been largely considered a star forming population inhabiting primarily low density environments (e.g. Brough et al. 2011; Bauer et al. 2013; Mahajan et al. 2015).

However, the structure of LBSs is at odds with these areas of apparent similarity to late types. LBSs are typically compact, with median effective radius of approximately one kpc (Kelvin et al. 2014), and Lange et al. (2016) have found that the mass versus size relation of LBSs was more likely compatible with Es than spirals.

Similarly in an analysis of 73 'blue spheroid' galaxies, visually classified with similar criteria to LBSs as compact, spheroidal, and blue but selected from a more nearby GAMA subsample ($z < 0.02$; ~60 per cent overlap with our LBS sample), Mahajan et al. (2018) find that blue spheroids show structural similarity to early-type
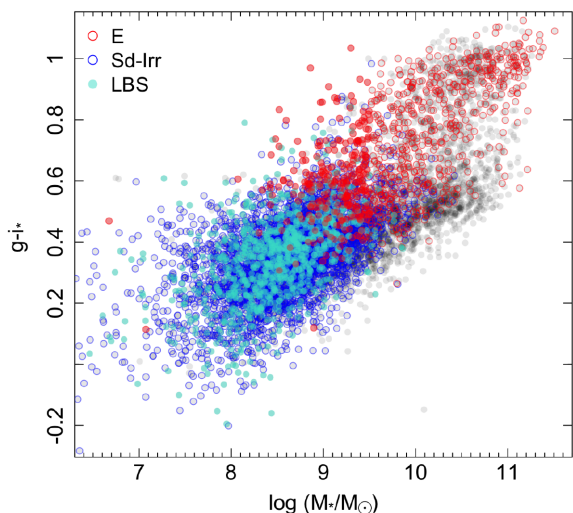
---

[1] GAMA-derived spectroscopic redshifts are assigned a normalized quality parameter (nQ) corresponding approximately to increasing confidence levels on the measurement, with 4 representing the highest quality and confidence level measurements. Standard practice within the survey is to require at least quality level 2 for use in scientific analysis.

[2] Note that an independent morphology classification performed by members of the SAMI Galaxy survey team also exists for a subset of these galaxies, and these independent classifications do not agree for all objects. The GAMA classifications are based on *giH* colour images compared to *gri* in the SAMI case, and SAMI classifications explicitly use signs of star formation as an indication of later type. These differences result in a tendency towards more later type classifications in the SAMI case (see Bassett et al. 2017 for a detailed discussion of these differences). Further, the SAMI classifications do not inlude a separate 'LBS' class, so the LBS sample that overlaps SAMI typically falls into late-type categories in the SAMI morphology classification.

Figure 2. GAMA Visual Morphology sample in colour versus stellar mass space, where $g - i_*$ is the intrinsic (corrected for internal dust extinction) $g - i$ colour from the SED modelling of Taylor et al. (2011). Stellar mass estimates are also derived from Taylor et al. (2011). Light grey points indicate the full sample distribution with coloured points indicating the E, Sd-Irr, and LBS classes. The subsample of 'low-mass E' galaxies is indicated in filled red points.

Figure 3. Distribution of LBS specific star formation rates compared to those of Sd-Irr and low-mass E galaxies, illustrating similar LBS and Sd-Irr star formation levels. The legend indicates p-values derived from K-S tests comparing the LBS property distribution to those of low-mass E (P_{ET}) and Sd-Irr (P_{LT}) populations.

Figure 4. Distribution of LBS mass-weighted ages compared to those of Sd-Irr and low-mass E galaxies, illustrating a tendency towards lower ages for LBSs compared to Sd-Irr and, much more significantly, low-mass E populations. The legend indicates p-values derived from K-S tests comparing the LBS property distribution to those of low-mass E (P_{ET}) and Sd-Irr (P_{LT}) populations.

galaxies along with stellar population properties more similar to late-type galaxies. Further, Mahajan et al. (2018) find that their blue spheroid galaxies follow the same star-formation rate versus atomic gas mass scaling relation as other star-forming galaxies and suggest that they could grow into spiral galaxies if supplied with sufficient gas accretion.

As illustrated in Fig. 2, nearly all LBSs in our sample lie at stellar masses below $10^{9.5}\,M_\odot$ (median stellar mass of the LBSs is $10^{8.5}\,M_\odot$). While this mass distribution is similar to that of the Sd-Irr class, it is clearly different from that of the full E class. As a result, when comparing the properties of LBSs to those of Es, we choose to specifically compare to the low-mass end of the E population (also known as dwarf elliptical or dE galaxies), which we select as those below $10^{9.5}$ in stellar mass (filled red points). Note that the LBS mass distribution does extend to lower stellar masses than the E population mass distribution. As a result, we also test a more restrictive mass selection that includes only those galaxies in the narrower mass overlap region of $10^{8.8}\,M_\odot < M_* < 10^{9.5}\,M_\odot$. When we redo comparisons between the three morphological classes using this selection, we find small differences in the exact values of test statistics we compute but no difference in the statistical significance of the results we report in the following sections.

In Fig. 3, we examine the GAMA-derived specific star formation rates (sSFRs) for LBSs compared to those of other visually classified late- and early-type galaxies. We use the stellar population fits to GAMA 21-band photometry (far-UV to far-IR) derived by Wright et al. (2016) using the MAGPHYS software (da Cunha, Charlot & Elbaz 2008), where sSFRS here are averaged over 10 Myr time-scales. We can see that, again, LBSs appear very similar to Sd-Irr galaxies in terms of star formation, with typical values of sSFR $\sim 10^{-10}\,yr^{-1}$ (cf. Bauer et al. 2013), where typical sSFRs for the low-mass E population is approximately an order of magnitude lower. Though typical LBS sSFR values are much more similar to the Sd-Irrs than Es, a Kolmogorov–Smirnov (K-S) test yields a <1 per cent chance that the LBS and Sd-Irr sSFRs are drawn from
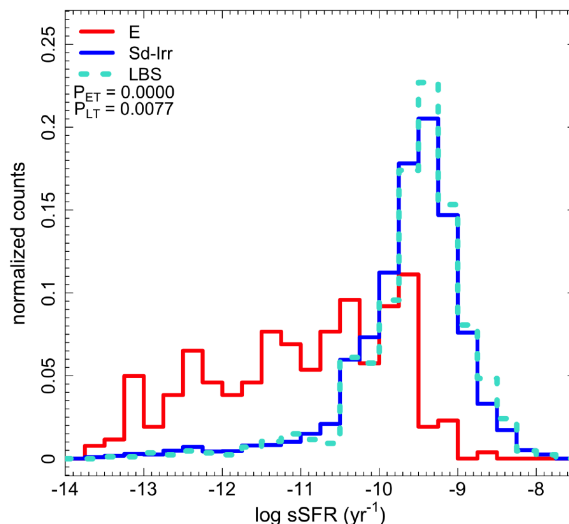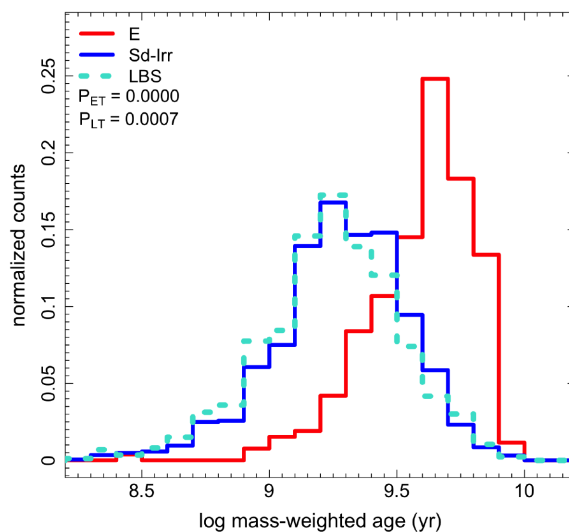
the same distribution. Note that while some of the LBS sSFRs are moderately high, they are generally not as extreme as other star forming dwarfs such as BCDs, which have SFRs ranging up to a few times $10\,M_\odot\,yr^{-1}$ (Hopkins, Schulte-Ladbeck & Drozdovsky 2002) compared to $<5\,M_\odot\,yr^{-1}$ for LBSs, or compact star forming galaxies, with sSFRs reaching over $10^{-8}\,yr^{-1}$ (Izotov et al. 2016). Thus if the high sSFR LBSs represent dwarf starbursts akin to BCDs, then the intensity of the star formation events appears to be lesser in LBSs.

Similarly in Fig. 4, we find that the median mass-weighted ages of the stellar population fits from MAGPHYS are similarly distributed
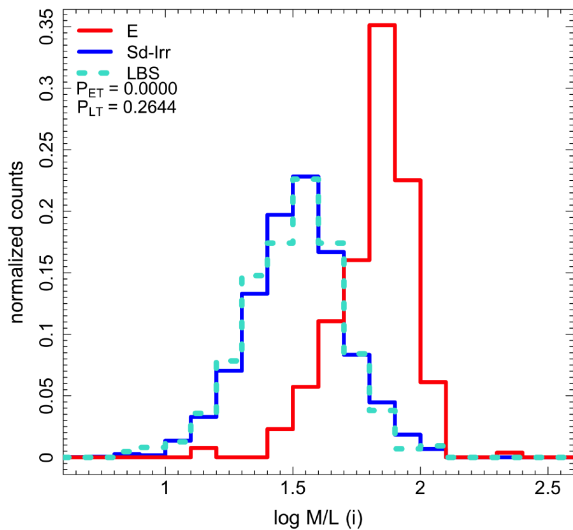
Figure 5. Distribution of LBS *i*-band mass-to-light ratios compared to those of Sd-Irr and low-mass E galaxies, illustrating that LBS and Sd-Irr mass-to-light ratio distributions are indistinguishable. The legend indicates p-values derived from K-S tests comparing the LBS property distribution to those of low-mass E (P_{ET}) and Sd-Irr (P_{LT}) populations.
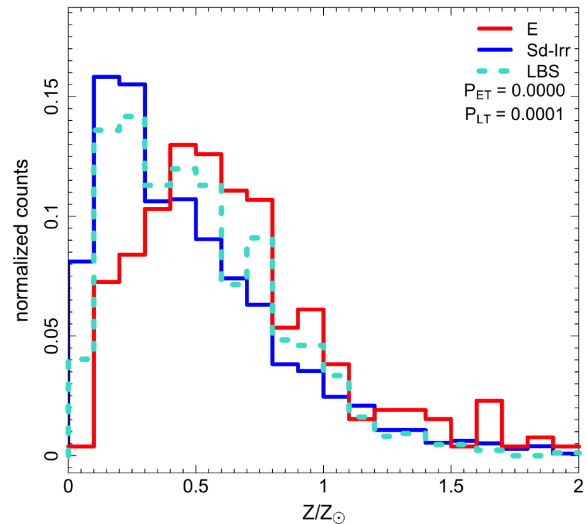

Figure 6. Distribution of LBS metallicities compared to those of Sd-Irr and low-mass E galaxies, illustrating that the LBS metallicity distribution skews higher than the Sd-Irr distribution but lower than the low-mass E distribution. The legend indicates p-values derived from K-S tests comparing the LBS property distribution to those of low-mass E (P_{ET}) and Sd-Irr (P_{LT}) populations.

between LBSs and Sd-Irrs, with low-mass Es shifted to significantly higher ages. In fact, LBSs have a tendency towards slightly lower typical ages than Sd-Irrs, and the K-S test probability that these populations are drawn from the same distribution is <1 per cent. We can also see a similar effect in the *i*-band mass-to-light ratios (Taylor et al. 2011) for the three populations in Fig. 5. Here LBSs and Sd-Irrs appear similar but disparate from the Es, which have a much higher mass-to-light ratios due to their older (hence faded) stellar populations. K-S test probabilities reinforce that the LBS and Sd-Irr mass-to-light ratio distributions are indistinguishable, while the E distribution is formally distinct. Using the MAGPHYS results again, we examine the metallicity distributions of the three groups in Fig. 6. There are sizeable errors in individual metallicity estimates here, so we cannot confidently distinguish a trend in the median metallicities for each class, however we do find that the LBS and Sd-Irr metallicity distributions are unlikely to be drawn from the same distribution (K-S probability <1 per cent).

Finally, we compare the local environments of LBSs to Sd-Irr and low-mass E galaxies. Fig. 7 illustrates the distribution of group halo masses derived from the GAMA survey group catalogue of Robotham et al. (2011). LBS and Sd-Irr group halo mass distributions are clearly more similar than the low-mass E distribution, which is significantly shifted towards higher mass haloes as is generally expected for dE galaxies (e.g. Sandage, Binggeli & Tammann 1985). A K-S test reveals an approximately 1 per cent chance that the LBS and Sd-Irr group halo mass distributions are drawn from the same population. Note that not all GAMA galaxies are associated with groups in this catalogue; those that do not lie in identified groups are considered 'isolated.' Only about 35 ± 3 per cent of the low-mass E galaxies are considered isolated by this metric, while 58 ± 1 per cent of Sd-Irr and 65 ± 1.5 per cent of LBS galaxies are isolated. From this GAMA group catalogue, we can also investigate the pair fractions of each galaxy class, with pairs defined by a projected physical separation of $100 \, \mathrm{kpc} \, h^{-1}$ or less and a velocity separation of $1000 \, \mathrm{km \, s^{-1}}$ or less. We find an approximately 27 ± 1.5 per cent pair fraction among LBSs with this metric, while Sd-Irr galaxies have a slightly higher 32 ± 1 per cent
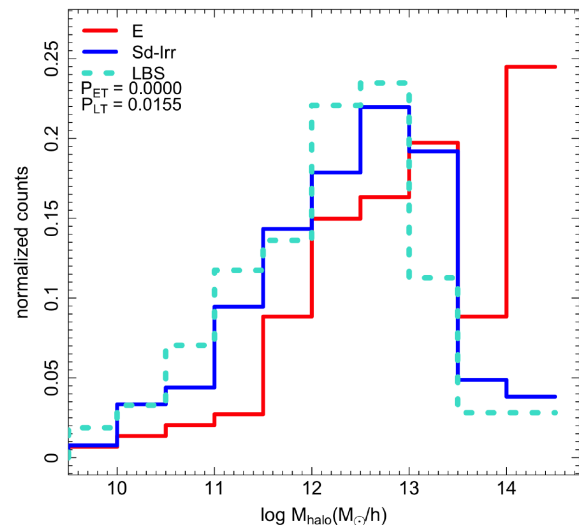

Figure 7. Distribution of LBS group halo masses compared to those of Sd-Irr and low-mass E galaxies, where LBSs tend to inhabit lower group halo mass environments than low-mass E galaxies and potentially slightly lower group halo mass environments than Sd-Irr galaxies as well. The legend indicates p-values derived from K-S tests comparing the LBS property distribution to those of low-mass E (P_{ET}) and Sd-Irr (P_{LT}) populations.

pair fraction. Thus, in general LBSs appear to occupy slightly lower density environments than even the relatively poor environments typical of Sd-Irrs.

4 LBS GALAXY STRUCTURE

We now compare the structure of LBS galaxies with Sd-Irr and low-mass E galaxies using structural parameters derived from photometric fits to VST KiDS survey (de Jong et al. 2013; de Jong et al. 2015; de Jong et al. 2017) *r*-band images.

4.1 PROFIT model fits

We make use of the Bayesian 2D profile-modelling code PROFIT (Robotham et al. 2017) and a series of automated wrapper codes to perform the necessary preparatory steps to running PROFIT on an input list of GAMA galaxies. PROFIT is open source (available at github.com/ICRAR/ProFit) and flexible with the ability to model a wide variety of standard model profiles and to employ an array of user-selected optimization algorithms.

To create the input images for PROFIT, we begin with calibrated, pipeline-processed *r*-band images from the VST KiDS survey data releases (de Jong et al. 2015; de Jong et al. 2017). We then apply additional processing steps as follows. We create an initial 400 arcsec on a side cutout image (and matching VST KiDS mask image containing pipeline data quality flags) and apply a local background subtraction to the cutout image based on the LAMBDAR (Wright et al. 2016) background subtraction procedure. We then derive an empirical PSF from the background subtracted image using PSFEx (Bertin 2011). We then create a reduced-size cutout image centred on the target galaxy (sized at three times the GAMA aperture radius for each galaxy) and a matching segmentation mask of objects in the frame detected with Source Extractor (Bertin & Arnouts 1996).

We next use PROFIT to obtain a single Sérsic model fit for each object, with initial parameter guesses derived from the GAMA aperture catalogue (Wright et al. 2016). We fit for the centre *x* and *y* pixel positions, total magnitude, r_e, Sérsic index (n), position angle, and axial ratio parameters of each single Sérsic model, with the r_e, n, and axial ratio parameters fit in log space. We use the centre coordinates, position angle, and axial ratio of each galaxy's GAMA catalogue aperture as our initial guess on the model's centre position, orientation, and axial ratio. Our initial guess for r_e is one sixth of the major axis radius of the GAMA aperture, and our initial guess for the total magnitude is the SDSS DR7 catalogue (Abazajian et al. 2009) petrosian *r*-band magnitude. We also set the initial guess on the Sérsic index equal to one. In general, these parameter guesses are somewhat arbitrary, but we structure our fitting procedure to limit sensitivity to initial guesses through use of Markov chain Monte Carlo (MCMC) sampling. We next perform an initial coarse optimization using the R optim function with the 'L-BFGS-B' algorithm. The results of this fit are used to provide improved initial guesses to the *LaplacesDemon*[3] package, which is used in MCMC mode, with the Component-wise Hit-And-Run Metropolis (CHARM) method, to find the most likely model over at least 10^4 iterations. The CHARM sampling algorithm was selected for its ability to sample across distant points in parameter space and perform well even in the presence of multimodal parameter distributions. We estimate parameter values and uncertainties only from the final stationary sample distributions, discarding up to 5000 iterations from the burnin phase, otherwise no explicit pruning of chains was performed. We also check that acceptance rates are considered suitable for our algorithm.

Finally, at the conclusion of the single Sérsic fits for each galaxy, we use the outputs of the single Sérsic fits to prepare initial parameter guesses for a double Sérsic model fitting run. Here we fit for the shared centre position of both components plus bulge and disc magnitudes, radii, position angles, and axial ratios. We also fit for the bulge *n* parameter but fix the disc *n* equal to one. We use the single Sérsic model fit centre and position angle as initial guesses for the corresponding parameter in both components. In general for

our sample that is numerically dominated by low-mass galaxies, we find that the single-component fit most often traces a discy galaxy component, so we use the total magnitude of the single fit as the initial guess for the disc component magnitude and half of this flux as the initial guess for the bulge component. Similarly, we use the single r_e as the initial guess for the disc radius and half this value as the initial guess for the bulge radius. We use twice the single *n* value as the guess for the bulge *n* value. We also use an initial axial ratio value for the bulge equal to one and the single fit value as the initial guess for the axial ratio of the disc component. We then calculate the most likely double Sérsic model according to the same fitting procedure as in the single Sérsic case.

Using this procedure, we have performed single and double Sérsic fits (in the KiDS *r* band) for all of the GAMA galaxies classified as 'little blue spheroid' from the GAMA II visual morphology catalogue (Moffett et al. 2016a) plus all GAMA galaxies that overlap with the public SAMI Galaxy survey sample target list (3159 objects in total; see example LBS fits in Fig. 8). Of these, fits for 419 galaxies initially failed because all galaxy pixels were within a masked region determined by the KiDS team (typically due to proximity to a bright star or its reflected light halo). For these initially failed fits, we found that many of these objects appear sufficiently uncontaminated that fits are possible, although some caution is necessary in interpreting the derived parameters. We subsequently fit these galaxies by providing an altered, no-masked-pixel mask image to PROFIT, and results from this analysis indicate that the majority of these objects can be reasonably well fit with this approach. However, we do assign such galaxies a quality flag indicating possibly compromised fits. For 94 objects found to have bad segmentation masks through visual inspection, an alternative solution of creating segmentation masks based directly on GAMA catalogue aperture positions has been attempted. Through visual inspection of the resulting fits, we find that some 80 per cent of these objects are recoverable with reasonable fits through this approach, however again we flag all such fits as potentially compromised in quality.

As a cross check on our derived structural parameters, we compare to the prior GAMA structural fitting results of Lange et al. (2016), based on shallower, lower resolution SDSS imaging, in Fig. 9. For overlapping objects between these two samples the single Sérsic fit parameters are in reasonably good agreement overall, however small systematic offsets in the derived radii and ellipticity values are apparent. Since these analyses were derived from different image sources (SDSS and VST KiDS), it is plausible that these differences result from imperfections in the empirically derived PSFs between sources. However, because in the following analysis we only interpret these results comparatively within one set of data, any systematics between data sources should not affect these comparative results. Further, our results on the structure of LBS galaxies are qualitatively consistent with those derived using the earlier Lange et al. (2016) GALFIT-based structural fits.

4.2 Structural model fit results

We now use these 2D model fits to investigate the detailed structure of the LBS galaxies. Note that although galaxies are complex and, in many cases, multicomponent structures, in light of the extra parameter degeneracies inherent in multicomponent modelling and the difficulty of deciding how many components are required for a satisfactory fit in an automated manner, we choose to focus here on our most stably measured single-component equivalent
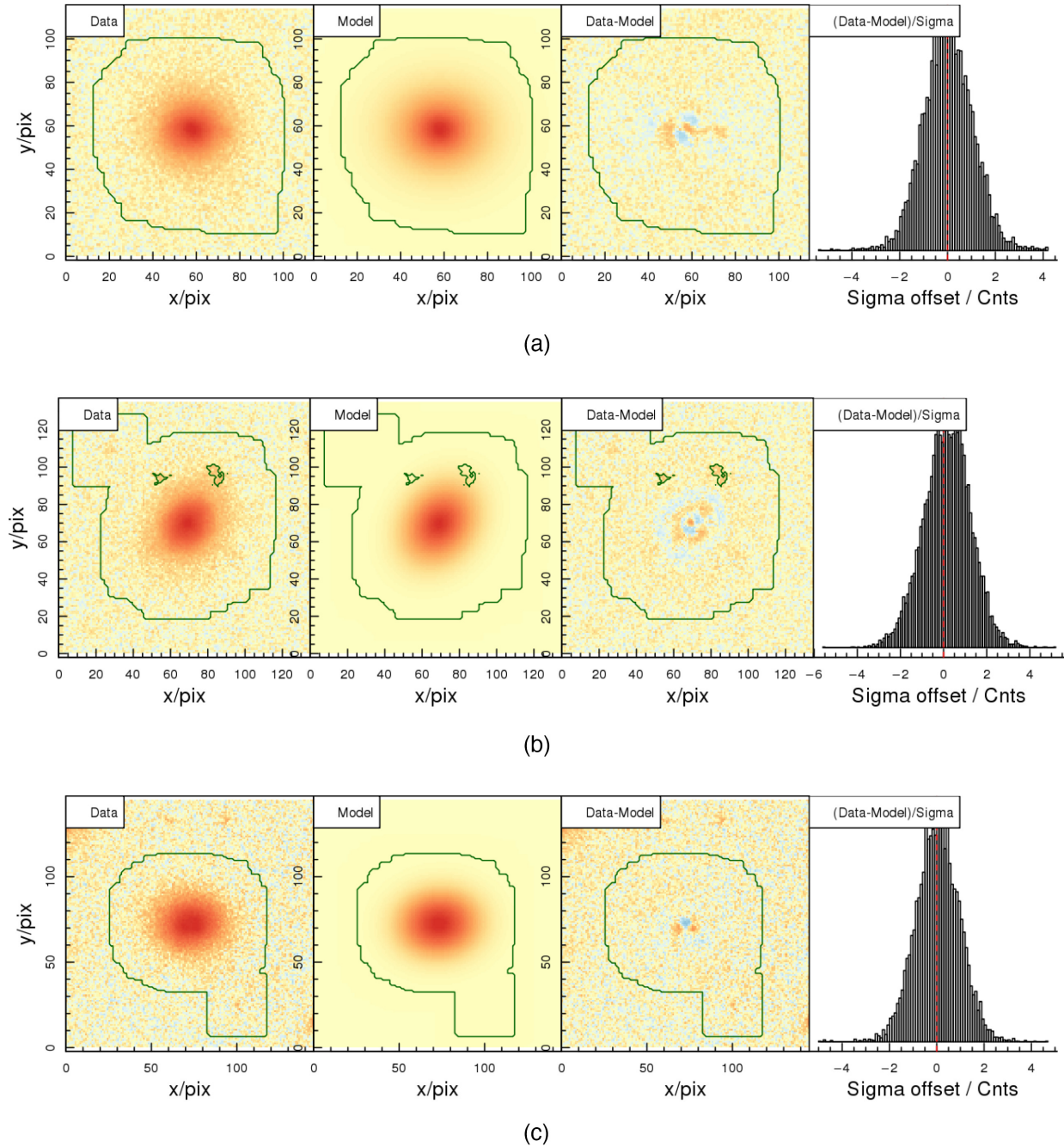
---

[3]https://github.com/LaplacesDemonR/LaplacesDemon

Figure 8. Example of PROFIT single Sérsic fits to VST KiDS *r*-band images of the galaxies shown in Fig. 1. Column one shows the data image, column two shows the selected model, column three shows a difference image, and column four shows a histogram of the residuals. The green contour indicates the fitting region derived from a Source Extractor image segmentation.

parameter values as a basis for comparison between the populations under consideration. Fig. 10 illustrates the *r*-band single Sérsic *n* distributions of LBS, Sd-Irr, and low-mass E galaxies. We find that LBSs have a similar Sérsic index distribution to that of low-mass Es. Although the LBS distribution appears to skew slightly lower, the median Sérsic *n* value for these two classes is consistent within uncertainties (1.63 ± 0.6 versus 1.69 ± 0.6 for LBSs and Es, respectively). On the other hand, the LBS *n* distribution skews higher than that of Sd-Irr galaxies, which have a median *n* of 0.94 ± 0.3 (i.e. steeper radial profiles), and K-S test results also emphasize that these distributions differ significantly. However,

comparing with a common early-/late-type divider used for giant galaxies, approximately 86 per cent of LBSs have Sérsic $n < 2.5$, which would typically be associated with discs or late types, and the other $\sim$14 per cent have $n > 2.5$, which would typically be associated with bulges or early types. We check that the Sérsic values for the low-mass E sample matches the expectation for classical dE galaxies from the Virgo Cluster. It is well known that *n* decreases with decreasing luminosity (e.g. Young & Currie 1994; Graham & Guzmán 2003), and most Virgo dEs in our luminosity/mass range have *n* between 0.5 and 3 (e.g. Gavazzi et al. 2005), consistent with typical values for both our low-mass Es and LBSs.
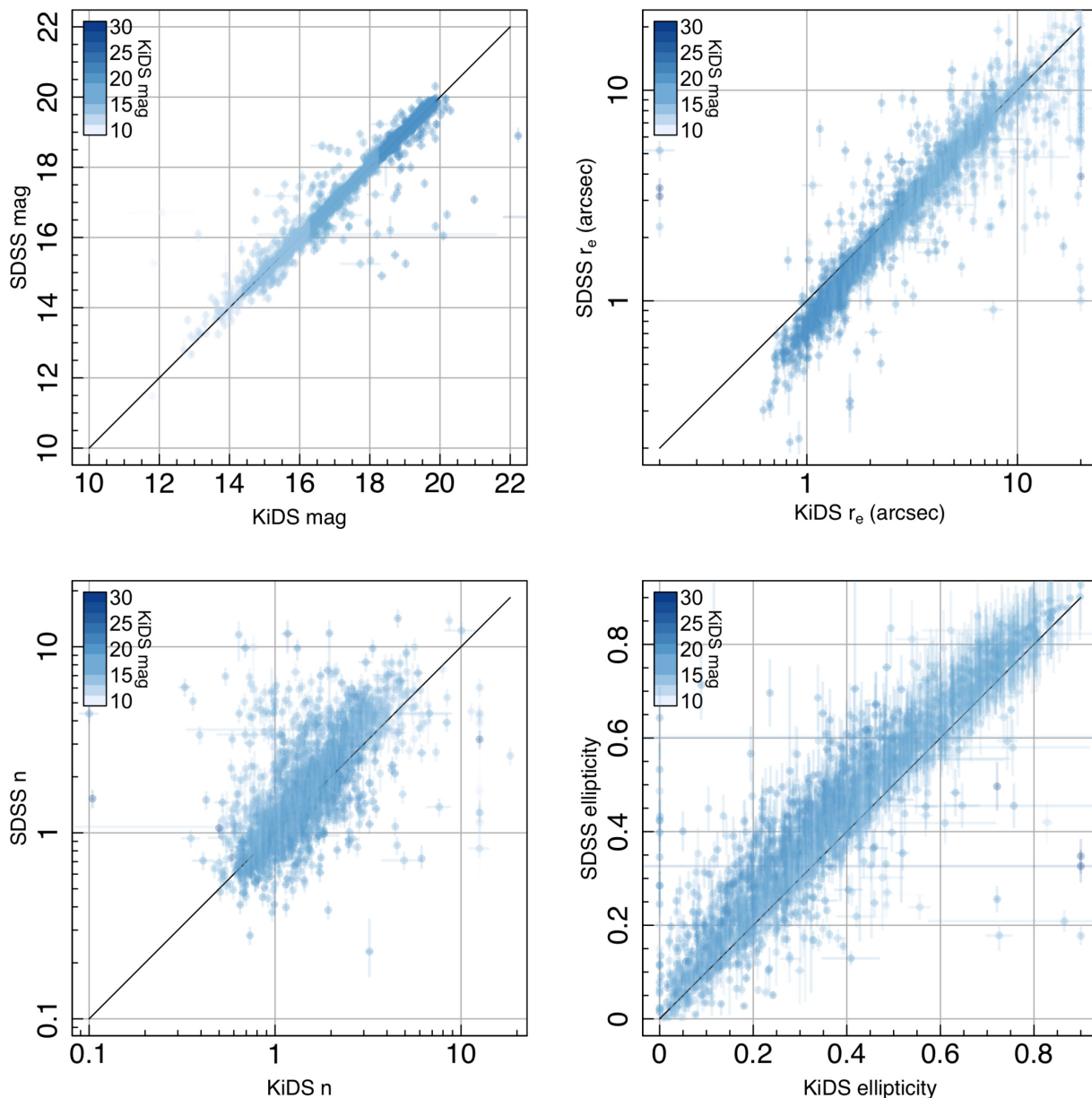
Figure 9. Comparison of single Sérsic fit parameters derived from PROFIT with VST KiDS imaging (current work) and GALFIT with SDSS imaging (Lange et al. 2016). In general, there is a close correspondence between PROFIT/KiDS and GALFIT/SDSS results, although a slight tendency towards smaller measured size and lower ellipticity is seen in the PROFIT/KiDS analysis.

Fig. 11 illustrates the size distributions of three classes, where the LBS population skews to smaller r_e than either Sd-Irrs or low-mass Es (K-S probability <1 per cent for LBS compatibility with either distribution). However, LBSs have a median r_e of ∼1 kpc, which is consistent with the median r_e of low-mass Es within uncertainties. We can also see in Fig. 12 that consistent with the morphological impression of spheroidal shape, the axial ratio (b/a) distribution of LBSs appears more similar to that of low-mass Es than to the Sd-Irrs (K-S probability <1 per cent for LBS compatibility with Sd-Irr distribution but ∼1 per cent for low-mass E distribution). We see that Sd-Irr galaxies have the widespread of axial ratios, with median ≃0.5, expected of a disc population (cf. Sandage, Freeman & Stokes 1970; Alam & Ryden 2002), while the spread of LBS axial ratios appears lower. The median b/a for LBSs is also consistent with that

of low-mass Es within uncertainties (0.74 ± 0.13 and 0.80 ± 0.17 for LBSs and Es, respectively).

Thus we confirm the incongruous results that LBSs have stellar population properties similar to Sd-Irr galaxies but structural properties that are compatible with low-mass Es. As the ellipticity measures only 2D shapes, one plausible option at this point might be that, rather than being a true spheroidal population, LBSs are just near face-on late types, perhaps with only a low level of irregularity and a more centrally peaked profile than usual, which are unneccessarily selected out as a separate class. To test this idea, we check that the Sd-Irr class does not seem to be lacking round images compared to the Sab-Scd class and find that adding the Sd-Irr and LBS classes would give an overall mean ellipticity lower than that of Sab-Scds (i.e. early-type spirals would be less round
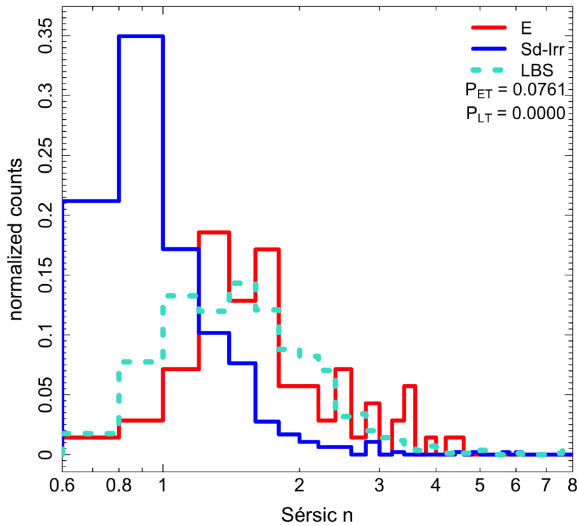
Figure 10. Distribution of LBS single Sérsic *n* values compared to Sd-Irr and low-mass E galaxies, illustrating that the LBS Sérsic *n* distribution is most similar to that of low-mass Es, albeit somewhat skewed to lower values. The legend indicates *p*-values derived from K-S tests comparing the LBS property distribution to those of low-mass E (P_{ET}) and Sd-Irr (P_{LT}) populations.
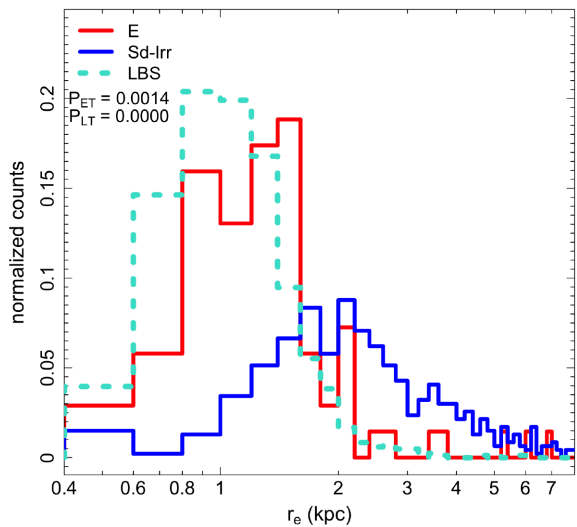

Figure 11. Distribution of LBS effective radius values (in kpc) compared to Sd-Irr and low-mass E galaxies, illustrating that the LBS effective radius distribution is similar to that of low-mass Es with a slight skew towards smaller size. The legend indicates p-values derived from K-S tests comparing the LBS property distribution to those of low-mass E (P_{ET}) and Sd-Irr (P_{LT}) populations.

than late-type spirals, which seems unlikely). We have also checked that Sd-Irr galaxies with higher values of *n* have the same ellipticity distribution as those with lower *n* (and hence still different to the LBSs).

Since LBS galaxies were originally morphologically classified from SDSS data, our deeper VST KiDS imaging offers the opportunity to identify any lower surface brightness features that may have been poorly detected at SDSS depth. We do find some examples of LBSs with more obvious two-component structure in this new imaging data set, and to quantify this, we consider a
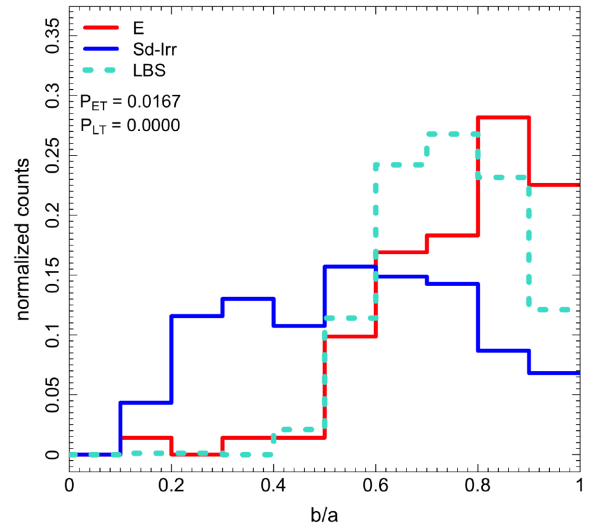
Figure 12. Distribution of LBS axial ratios compared to Sd-Irr and low-mass E galaxies, illustrating that the LBS axial ratio distribution is more similar to low-mass Es than Sd-Irrs. The legend indicates p-values derived from K-S tests comparing the LBS property distribution to those of low-mass E (P_{ET}) and Sd-Irr (P_{LT}) populations.

likelihood ratio test with the null hypothesis that the single Sérsic model is a good description for each galaxy. We then calculate the probability of this null hypothesis according to a chi-square distribution with degrees of freedom given by the difference in degrees of freedom between the two models. If this probability is <5 per cent, we consider the double Sérsic model to be preferable. We find that this metric implies ~85 per cent of LBSs are better represented by two-component models. By this same metric, we find that only ~30 per cent of our low-mass E sample would be best described by two-component models (previous observations of dwarf early types with embedded disc components include the works of e.g. Jerjen, Kalnajs & Binggeli 2000; Barazza, Binggeli & Jerjen 2002; De Rijcke et al. 2003; Geha, Guhathakurta & van der Marel 2003; Graham & Guzmán 2003). Thus, the more common presence of disc components in LBS galaxies may be responsible for the small differences in structural parameters compared to low-mass E galaxies, and we investigate the possibility of disc-like structure in LBSs further through consideration of their kinematics in the next section.

5 SAMI KINEMATICS OF LBSS

We now examine the SAMI Galaxy survey integral field kinematics for LBS galaxies with data available in SAMI Data Release 2 (Scott et al. 2018). The SAMI survey selection is primarily drawn from GAMA, and there are 62 LBS galaxies that have emission line data of sufficient quality for spatially resolved kinematic analysis available in SAMI data release 2. For comparison, we also consider a sample of elliptical galaxies (20) and Sd-Irr galaxies (60) from our GAMA morphology sample with similar masses to the LBS sample and high-quality emission line data available from SAMI. These emission line data are processed using the LZIFU (Ho et al. 2016) line fitting procedure described by Green et al. (2018) and Medling et al. (2018). We use the velocity maps derived from this analysis to extract rotation curves along each galaxy's major axis position angle, which we determine using the kinematry methods of Krajnović et al. (2006). Note that each SAMI velocity field covers
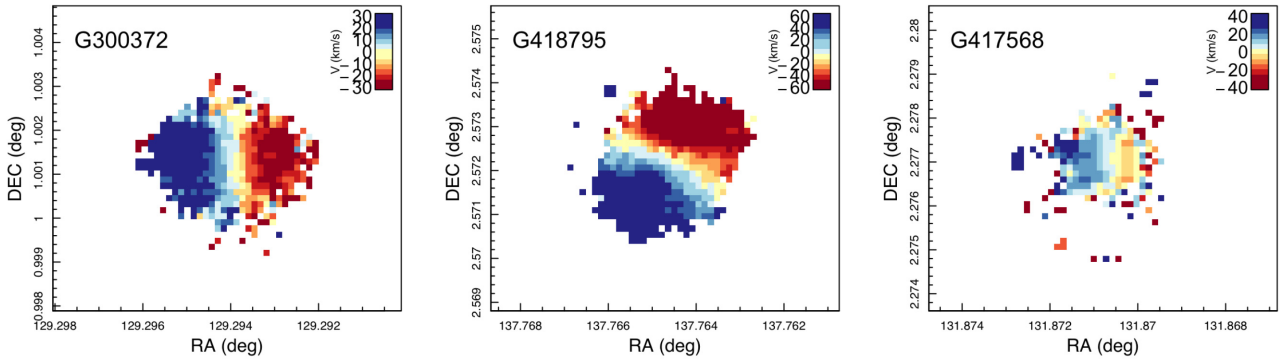
Figure 13. SAMI emission line velocity maps derived from the analysis described by Green et al. (2018) and Medling et al. (2018). The left and middle panels show examples of LBS galaxies with velocity fields that display extended, regular rotation well fit by the symmetric rising rotation curve form used here, while the far right panel shows an example of an LBS velocity field that is poorly fit with this rotation curve form. Note that the category of galaxies that are poorly fit by a symmetric rising rotation curve (and for which we cannot obtain a reliable characteristic rotation velocity with this method) includes both objects with some evidence of disturbed rotation (as in the far right panel above) and those with no apparent rotation signature. We omit spaxels with large measured velocity errors (>15 km s^{-1}) from the plotted maps.

a footprint ~ 15 arcsec in diameter, which for the median size of our LBS galaxies covers out to $\sim 5 r_e$. We fit the derived 1D rotation curves using the following simple piecewise functional form for velocity as a function of radius (e.g. Wright et al. 2007; Epinat et al. 2009):

$$V(r) = \begin{cases} V_t \times (r/r_t) & r \leq r_t \\ V_t & r > r_t. \end{cases}$$

For comparison, we also use SAMI stellar kinematics measurements (van de Sande et al. 2017b), specifically the stellar velocity dispersion values measured within elliptical r_e derived using the Multi-Gaussian Expansion method (MGE; Emsellem, Monnet & Bacon 1994; Cappellari 2002) and code from Scott et al. (2009) applied to GAMA imaging (d'Eugenio, private communication). We note that comparing rotational velocity derived from ionized gas with stellar velocity dispersion is not necessarily standard practice since stars and gas may not trace the underlying potential in the same way, e.g. due to asymmetric drift. Here the decision to do so is largely a practical one; since the low-mass LBS galaxies are star forming, the emission line data provide superior S/N to trace the kinematics to large radii. Cortese et al. (2014) find the average relationship V_{rot}(stars)/V_{rot}(gas) is 0.75 for SAMI galaxies, and we find that a correction to our measured gas rotation velocities of this magnitude would not substantially change the following results.

Out of the 62 LBS galaxies with emission line kinematics maps, we can derive an ionized gas maximum circular velocity (V_{rot}) for 42 galaxies with this method. The remaining 20 LBSs have either ill-defined rotation axes or disturbed kinematics that are not well fit by the simple rising rotation curve form used here (see Fig. 13 for rotating and disturbed velocity field examples). Fig. 14(a) shows the derived ionized gas rotation velocity divided by stellar velocity dispersion (V_{rot}/σ) versus galaxy stellar mass for the LBSs and low-mass Es and Sd-Irrs with measurable rotation curves and measurable stellar velocity dispersion values as determined by Scott et al. (2018), totalling 31 LBSs, 13 low-mass Es, and 19 low-mass Sd-Irrs. Rotation velocities are inclination corrected based on estimating inclination from each galaxy's ellipticity and assuming intrinsic flattening of 0.3. Since the stellar velocity resolution of SAMI data is ~ 70 km s^{-1}, the σ values we derive for these low-mass galaxies typically represent upper limits, and we represent

these cases with arrows replacing their error bars in the V_{rot}/σ space. We find that both LBSs and low-mass Es with measurable rotation typically have V_{rot}/σ consistent with or greater than unity. In fact, the V_{rot}/σ distributions of all three morphological classes appear similar at these low masses, with the prevalence of limit values on σ in this data set making it problematic to determine whether or not any class has a significant offset in typical V_{rot}/σ.

Although we find that some of our LBSs have disturbed or not clearly rotating kinematics, the V_{rot}/σ values we derive for the others indicate that ~ 68 per cent of our LBS galaxies are at least marginally rotation-dominated systems. We find that a similar fraction of our low-mass Es are also rotation-dominated. Significant rotation has previously been observed in the *stellar* kinematics of early-type galaxies and, in particular, appears to be more common for low-mass early types (see e.g. Emsellem et al. 2007; Bassett et al. 2017; Brough et al. 2017; van de Sande et al. 2017a). It is also not surprising that Sd-Irr galaxies in this sample are typically found to be rotation dominated.

In Fig. 14(b), we further explore the characteristic rotation velocities for members of each class with measurable rotation. We see that at constant stellar mass, the Sd-Irr galaxies appear to have slightly larger V_{rot} values than LBS galaxies, with a <1 per cent K-S test probability that these populations are drawn from the same distribution. In contrast, LBS V_{rot} values appear to be more similar to those of low-mass E galaxies, however we cannot conclusively say these V_{rot} distributions are identical, as we find ~ 8 per cent K-S test probability that these populations are drawn from the same distribution.

6 DISCUSSION AND CONCLUSIONS

To summarize the results of the preceding sections, we find that the dwarf LBS galaxy class combines stellar population properties similar (although not identical) to spiral/irregular galaxies (including colours, specific star formation rates, stellar population ages, mass-to-light ratios, and metallicities) with morphology and structural properties (including Sérsic indices, radii, and axial ratios) compatible with low-mass elliptical galaxies. Further, LBSs typically occupy relatively poor environments similar to Sd-Irr galaxies but with an even greater tendency towards isolation. From analysis of SAMI kinematics of LBSs, we also find that the *majority*
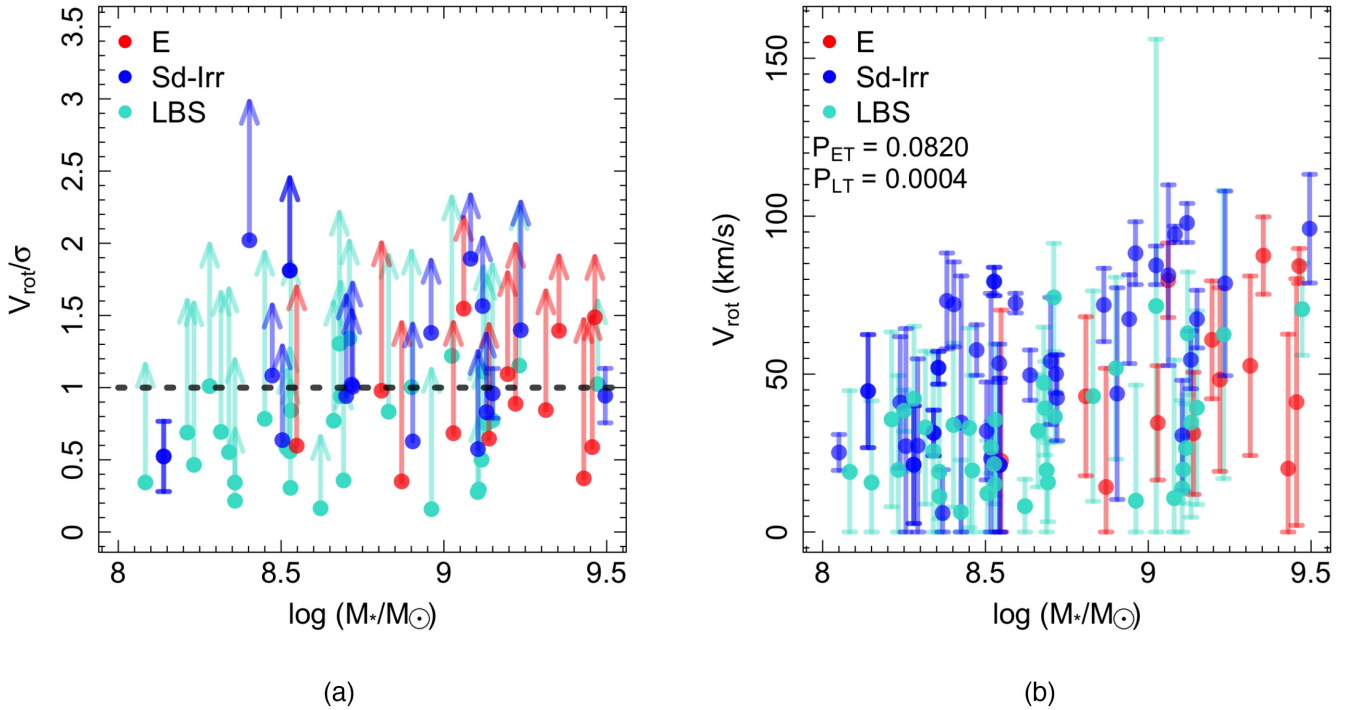
Figure 14. Panel a: SAMI-derived rotational velocity divided by velocity dispersion (V_{rot}/σ) versus stellar mass for LBS and low-mass E and Sd-Irr galaxies. Error bars are plotted as limit arrows where the SAMI stellar velocity resolution is greater than the measured velocity dispersion. The black dashed line indicates equal contribution from rotational velocity and velocity dispersion. LBSs and low-mass Es for which we can derive reliable rotation measures are typically consistent with or above this line, and as such we infer they are at least marginally rotation-dominated systems. Panel b: SAMI-derived, rotational velocities versus stellar mass for LBS and low-mass E and Sd-Irr galaxies. At constant stellar mass, Sd-Irr rotation velocities appear to be slightly higher than LBS and E velocities, which are more similar. The legend indicates p-values derived from K-S tests comparing LBS rotation velocities to those of the low-mass E (P_{ET}) and Sd-Irr (P_{LT}) samples.

of LBSs display at least marginally rotation-dominated dynamics, similar to low-mass ellipticals.

We first consider whether or not this population is a plausible star-forming, field-environment precursor to dwarf elliptical galaxies. We then discuss the overlap of this population with other compact, star-forming populations and the evolutionary processes that are potentially associated with such populations, including interactions/mergers, external gas accretion, and downsizing in galaxy formation.

Our PROFIT modelling analysis suggests that LBSs are structurally equivalent to dwarf elliptical galaxies but with ongoing star formation. In recent work, George (2017) has also found structural similarity between dwarf ellipticals and a 55-galaxy sample of SDSS star-forming, blue early-type galaxies. The star formation (history) of LBSs seems to be very similar to that in the equally low mass but disc-like faint Sd-Irr galaxies (which we can equate to dI galaxies). Adding in the fact that they live in similar low-density environments as dIs, we can then hypothesize that LBSs are field counterparts of cluster dEs. They have continued to form stars at a relatively constant rate (given that the inverse of their sSFR is of order 10^{10} yr) while their clustered cousins have largely ended their star formation much earlier. In turn this dichotomy suggests that, just as at high masses, there are two structural types of low-mass galaxy, spheroidal and disc-like, but that star formation continues in both types absent a quenching mechanism. Given their similar sSFRs to dwarf irregular galaxies, it seems likely that the LBSs have sufficient fuel to maintain substantial star formation for several more Gyr. Indeed, though we do not as

yet have gas masses for our LBS sample, Mahajan et al. (2018) do find that their blue spheroids (including many of our lowest redshift LBSs) display similar gas properties to star-forming disc galaxies.

If these LBSs were to decrease or end their star formation, we would expect them to move towards the region of the colour versus stellar mass diagrams occupied by low-mass Es (see Fig. 2). This would suggest that the progenitors of cluster dEs could be LBS-like objects and not dwarf irregulars, which could solve the long-standing problem of how to transform star forming dwarf irregulars to create the large cluster dE populations, given the differences in structure and surface density between the two classes (e.g. Davies & Phillips 1988; Meyer et al. 2014). As we have found here, LBSs already show strong structural similarity to low-mass Es, so quenching of star formation brought on by the effects of infall into a richer environment could be sufficient to make LBSs similar to dEs, whereas a structurally different dI would have to be both quenched and have its structure altered by environmental interaction. We find that most LBSs have significant rotational support and some low-mass Es also display similar kinematic properties, implying minimal change to the dynamical structure of LBSs would be required to transition into such low-mass Es. However, due to their previously discussed low density environments, it is unlikely that the currently observed LBSs will directly transform into their clustered dE cousins. Interestingly, Janz et al. (2017) has identified examples of isolated and quenched low-mass early-type galaxies with rotating kinematics, which suggests early-type dwarfs can also be quenched outside of rich environments.

Blue compact dwarf (BCD) galaxies have frequently been suggested as a progenitor population to dEs (e.g. Davies & Phillipps 1988; Meyer et al. 2014), and there is significant but not perfect overlap between LBSs and the typical colour, surface brightness, and magnitude range used to select BCDs (e.g. Gil de Paz et al. 2003). Morphologically there is also significant similarity between these galaxy types, with compact cores frequently surrounded by a lower surface brightness component. Like BCDs, star formation in our LBSs also appears primarily centrally concentrated, although extended disc star formation could remain undetected at the depth of our SAMI maps. LBSs also overlap with the luminous blue compact galaxy and Green Pea classifications in their compact, star-forming nature (e.g. Koo et al. 1994; Cardamone et al. 2009), however the typical LBS is less massive, less extremely star forming, and found at lower redshift than these populations.

Interactions between galaxies are a common explanation for the mixture of compact morphology and recent star formation observed in galaxies like BCDs (e.g. Telles & Terlevich 1995; Noeske et al. 2001; Pustilnik et al. 2001). Similarly, the blue E/S0 population of Kannappan et al. (2009) is strongly associated with interactions or mergers. More recently compact dwarf populations have been suggested as the likely products of *dwarf–dwarf* mergers that could both drive a central starburst and lead to disturbed kinematics in the remnant galaxy (e.g. Lelli et al. 2012; Ashley et al. 2014; Koleva et al. 2014). However, as previously noted, the typical star formation rates of LBSs are lower than those typical of BCDs, and only ∼10 per cent of our LBSs reach sSFRs compatible with starbursts. Within the stellar mass range most of our LBSs inhabit these galaxies make up ∼20 per cent of the galaxy population (Moffett et al. 2016a), and therefore the high sSFR tail represents only a few per cent of the low-mass population. Interestingly, this figure is similar to the ∼4 per cent major merger rate estimated at such low masses by Casteels et al. (2014), which seems to support the plausibility of a merger origin for such galaxies. Most other LBSs would then be expected to originate from events that would incite lower intensity star formation, possibly still including interactions or more minor merger events.

External gas accretion may also be an important ingredient in maintaining the star formation we observe in LBSs. Graham et al. (2017) consider in detail a case of an isolated dwarf early-type galaxy that closely overlaps the properties of our LBS class. In this galaxy, the authors find not only significant rotation but also gas and stellar components that are counter-rotating with respect to one another, strongly implying an external accretion origin for the galaxy's gas supply. External accretion that enables building of a new disc around an existing compact core appears to be a plausible process at work in LBS galaxies, particularly the ∼85 per cent of LBSs we find are best-fitting with an additional (typically disc-like) structural component.

Finally, LBSs could also potentially represent a downsized version of a galaxy population both predicted and observed at higher redshifts, the 'blue nuggets' (e.g. Barro et al. 2013; Dekel & Burkert 2014; Zolotov et al. 2015; Tacchella et al. 2016). The blue nugget population is believed to form through a process of gas compaction triggered by mergers or significant gas accretion. The products of this process are forming stars at a rate similar to the high end of the LBS distribution (sSFR ∼10^{-9} yr^{-1}) but are typically an order of magnitude higher in stellar mass with accordingly higher stellar mass surface density. Thus if created through similar processes, LBSs would have to represent a downsized (more recently formed and thus lower mass) version of this population.

In summary, we find that LBSs could plausibly emerge from a mixture of merger and accretion processes acting on the low-redshift dwarf galaxy population. These scenarios are not necessarily mutually exclusive, and our observed LBS population may well be a mixture of recent merger products, galaxies in currently isolated environments forming stars at a slow and steady pace, and galaxies with significant gas accretion building up a disc component. We also conclude that LBS galaxies resemble a non-quenched, field-environment counterpart to dEs, and if an LBS galaxy were to be subjected to larger scale environmental forces such as infall into a richer cluster environment, it would likely evolve into a product resembling a typical cluster dE. The kinematic diversity in LBS galaxies, from disturbed to regularly rotating, also gives us a clue to the likely spread of evolutionary processes affecting this population. In future work, we plan to use the growing survey samples of integral field kinematic data for galaxies extending into the low mass regime in order to better understand the link between the photometrically inferred structure and detailed kinematic characteristics of such galaxies.

REFERENCES

Abazajian K. N. et al., 2009, ApJS, 182, 543
Alam S. M. K., Ryden B. S., 2002, ApJ, 570, 610
Ashley T., Elmegreen B. G., Johnson M., Nidever D. L., Simpson C. E., Pokhrel N. R., 2014, AJ, 148, 130
Barazza F. D., Binggeli B., Jerjen H., 2002, A&A, 391, 823
Barro G. et al., 2013, ApJ, 765, 104
Bassett R. et al., 2017, MNRAS, 470, 1991
Bauer A. E. et al., 2013, MNRAS, 434, 209
Bertin E., 2011, in Evans I. N., Accomazzi A., Mink D. J., Rots A. H., eds, ASP Conf. Ser. Vol. 442, Astronomical Data Analysis Software and Systems XX. Astron. Soc. Pac., San Francisco, p. 435
Bertin E., Arnouts S., 1996, A&AS, 117, 393
Binggeli B., Sandage A., Tarenghi M., 1984, AJ, 89, 64
Brough S. et al., 2011, MNRAS, 413, 1236
Brough S. et al., 2017, ApJ, 844, 59
Bryant J. J. et al., 2015, MNRAS, 447, 2857
Buta R. J., 2013, Galaxy Morphology. Cambridge University Press, Cambridge. p. 1
Cappellari M., 2002, MNRAS, 333, 400
Cardamone C. et al., 2009, MNRAS, 399, 1191
Casteels K. R. V. et al., 2014, MNRAS, 445, 1157
Cole S., Lacey C. G., Baugh C. M., Frenk C. S., 2000, MNRAS, 319, 168
Colless M. et al., 2001, MNRAS, 328, 1039
Conselice C. J., 2003, ApJS, 147, 1
Cortese L. et al., 2014, ApJ, 795, L37
Croom S. M. et al., 2012, MNRAS, 421, 872
da Cunha E., Charlot S., Elbaz D., 2008, MNRAS, 388, 1595
Davies J. I., Phillipps S., 1988, MNRAS, 233, 553
Davies L. J. M. et al., 2016, MNRAS, 461, 458
de Jong J. T. A. et al., 2013, Messenger, 154, 44
de Jong J. T. A. et al., 2015, A&A, 582, A62
de Jong J. T. A. et al., 2017, A&A, 604, A134
De Rijcke S., Dejonghe H., Zeilinger W. W., Hau G. K. T., 2003, A&A, 400, 119
Dekel A., Burkert A., 2014, MNRAS, 438, 1870
Driver S. P. et al., 2006, MNRAS, 368, 414
Driver S. P. et al., 2009, Astron. Geophys., 50, 12
Emsellem E., Monnet G., Bacon R., 1994, A&A, 285, 723
Emsellem E. et al., 2007, MNRAS, 379, 401
Epinat B. et al., 2009, A&A, 504, 789
Faber S. M., Lin D. N. C., 1983, ApJ, 266, L17
Fall S. M., Efstathiou G., 1980, MNRAS, 193, 189
Ferguson H. C., Binggeli B., 1994, A&AR, 6, 67
Gavazzi G., Donati A., Cucciati O., Sabatini S., Boselli A., Davies J., Zibetti S., 2005, A&A, 430, 411
Geha M., Guhathakurta P., van der Marel R. P., 2003, AJ, 126, 1794
George K., 2017, A&A, 598, A45
Gil de Paz A., Madore B. F., Pevunova O., 2003, ApJS, 147, 29
Graham A. W., Guzmán R., 2003, AJ, 125, 2936
Graham A. W., Janz J., Penny S. J., Chilingarian I. V., Ciambur B. C., Forbes D. A., Davies R. L., 2017, ApJ, 840, 68
Green A. W. et al., 2018, MNRAS, 475, 716
Hill D. T. et al., 2011, MNRAS, 412, 765
Ho I.-T. et al., 2016, Ap&SS, 361, 280
Hopkins A. M., Schulte-Ladbeck R. E., Drozdovsky I. O., 2002, AJ, 124, 862
Hopkins A. M. et al., 2013, MNRAS, 430, 2047
Huertas-Company M. et al., 2015, ApJS, 221, 8
Huxor A. P., Phillipps S., Price J., 2013, MNRAS, 430, 1956
Izotov Y. I., Guseva N. G., Fricke K. J., Henkel C., 2016, MNRAS, 462, 4427
Janz J., Penny S. J., Graham A. W., Forbes D. A., Davies R. L., 2017, MNRAS, 468, 2850
Jerjen H., Kalnajs A., Binggeli B., 2000, A&A, 358, 845
Kannappan S. J., Guie J. M., Baker A. J., 2009, AJ, 138, 579
Kelvin L. S. et al., 2014, MNRAS, 439, 1245
Koleva M., De Rijcke S., Zeilinger W. W., Verbeke R., Schroyen J., Vermeylen L., 2014, MNRAS, 441, 452
Koo D. C., Bershady M. A., Wirth G. D., Stanford S. A., Majewski S. R., 1994, ApJ, 427, L9
Krajnović D., Cappellari M., de Zeeuw P. T., Copin Y., 2006, MNRAS, 366, 787
Lange R. et al., 2016, MNRAS, 462, 1470
Lelli F., Verheijen M., Fraternali F., Sancisi R., 2012, A&A, 537, A72
Lintott C. et al., 2011, MNRAS, 410, 166
Liske J. et al., 2015, MNRAS, 452, 2087
Loose H. H., Thuan T. X., 1986, in Kunth D., Thuan T. X., Van J. T. T., eds, Star-forming Dwarf Galaxies and Related Objects, Editions Frontières in Gif sur Yvette, France, p. 73
Lotz J. M., Primack J., Madau P., 2004, AJ, 128, 163
Mahajan S. et al., 2015, MNRAS, 446, 2967
Mahajan S. et al., 2018, MNRAS, 475, 788
Medling A. M. et al., 2018, MNRAS, 475, 5194
Meyer H. T., Lisker T., Janz J., Papaderos P., 2014, A&A, 562, A49
Moffett A. J. et al., 2016a, MNRAS, 457, 1308
Moffett A. J. et al., 2016b, MNRAS, 462, 4336
Noeske K. G., Iglesias-Páramo J., Vílchez J. M., Papaderos P., Fricke K. J., 2001, A&A, 371, 806
Pustilnik S. A., Kniazev A. Y., Lipovetsky V. A., Ugryumov A. V., 2001, A&A, 373, 24
Robotham A. S. G. et al., 2011, MNRAS, 416, 2640
Robotham A. S. G., Taranu D. S., Tobar R., Moffett A., Driver S. P., 2017, MNRAS, 466, 1513
Sandage A., Binggeli B., 1984, AJ, 89, 919
Sandage A., Freeman K. C., Stokes N. R., 1970, ApJ, 160, 831
Sandage A., Binggeli B., Tammann G. A., 1985, AJ, 90, 1759
Schawinski K. et al., 2009, MNRAS, 396, 818
Scott N. et al., 2009, MNRAS, 398, 1835
Scott N. et al., 2018, MNRAS, 481, 2299
Tacchella S., Dekel A., Carollo C. M., Ceverino D., DeGraf C., Lapiner S., Mandelker N., Primack Joel R., 2016, MNRAS, 457, 2790
Taylor E. N. et al., 2011, MNRAS, 418, 1587
Telles E., Terlevich R., 1995, MNRAS, 275, 1
Thuan T. X., Martin G. E., 1981, ApJ, 247, 823
van de Sande J. et al., 2017a, MNRAS, 472, 1272
van de Sande J. et al., 2017b, ApJ, 835, 104
Willett K. W. et al., 2013, MNRAS, 435, 2835
Wright S. A. et al., 2007, ApJ, 658, 78
Wright A. H. et al., 2016, MNRAS, 460, 765
York D. G. et al., 2000, AJ, 120, 1579
Young C. K., Currie M. J., 1994, MNRAS, 268, L11
Zolotov A. et al., 2015, MNRAS, 450, 2327

[1]*Department of Physics and Astronomy, Vanderbilt University, PMB 401807 2401 Vanderbilt Place, Nashville TN 37240, USA*

[2]*Department of Physics and Astronomy, University of North Georgia, 3820 Mundy Mill Rd., Oakwood GA 30566, USA*

[3]*School of Physics, University of Bristol, Tyndall Avenue, Bristol BS8 1TL, UK*

[4]*ICRAR, The University of Western Australia, 35 Stirling Highway, Crawley WA 6009, Australia*

[5]*ARC Centre of Excellence for All Sky Astrophysics in 3 Dimensions (ASTRO 3D)*

[6]*School of Physics, University of New South Wales, NSW 2052, Australia*

[7]*School of Physics and Astronomy, Monash University, VIC 3800, Australia*

[8]*Sydney Institute for Astronomy, School of Physics, A28, The University of Sydney, NSW 2006, Australia*

[9]*Australian Astronomical Optics, 105 Delhi Rd, North Ryde, NSW 2113, Australia*

[10]*School of Physics and Astronomy, University of Nottingham, Nottingham NG7 2RD, UK*

[11]*Indian Institute of Astrophysics, 2nd Block, Koramangala, Bangalore 560034, India*

[12]*Department of Physics, Christ University, Hosur Road, Bangalore 560029, India*

[13]*Department of Physics and Astronomy, Macquarie University, NSW 2109, Australia*

[14]*Department of Physics and Astronomy, 102 Natural Science Building, University of Louisville, Louisville KY 40292, USA*

[15]*Australian Astronomical Optics, Macquarie University, 105 Delhi Rd, North Ryde, NSW 2113, Australia*

[16]*Atlassian, 341 George St Sydney, NSW 2000, Australia*

[17]*Ritter Astrophysical Research Center, University of Toledo, Toledo, OH 43606, USA*

[18]*Research School for Astronomy and Astrophysics, Australian National University, Canberra, ACT 2611, Australia*

[19]*E. A. Milne Centre for Astrophysics, University of Hull, Cottingham Road, Kingston-upon-Hull, HU6 7RX, UK*

[20]*SOFIA Science Center, USRA, NASA Ames Research Center, Building N232, M/S 232-12, P.O. Box 1, Moffett Field, CA 94035-0001, USA*

[21]*Centre for Astrophysics and Supercomputing, Swinburne University of Technology, PO Box 218, Hawthorn, VIC 3122, Australia*

This paper has been typeset from a TeX/LaTeX file prepared by the author.